Modelling of a Gerotor pump including the evaluation of the micro-movements of the external gear

Modelling of a Gerotor pump including the evaluation of the micro-movements of the external gear

G Totaro[1], B Zardin[1,a], M Borghi[1], F Scolari[2]

[1]Engineering Department Enzo Ferrari DIEF, via P. Vivarelli 10, 41125 Modena Italy
[2]CNH Industrial Italia SpA, viale delle Nazioni 55, 41122 Modena Italy
[a] barbara.zardin@unimore.it

Abstract. Gerotor pumps are positive displacement pumps used in many applications thanks to their compact size and low cost. On the other side the efficiency of the machine is not so brilliant. In order to study design modifications to decrease energy consumption, a lumped parameter model is a useful tool since it allows predicting and enhancing pump performance. This type of model can be used, once complete, to analyse various phenomena such as cavitation, the chambers' pressure transient, the flow and pressure ripple, the leakages, and the noise emissions. This work presents a lumped parameter model for the analysis of a Gerotor pump, including the evaluation of the micro movements of the external gear. These micro-movements potentially affect the gap geometry at the internal gear tooth tips and have an impact on the pump's performance. We modelled the behaviour of the external gear as a journal bearing under dynamic load and then we compared various methods to solve the problem and to find the most suitable method to be coupled with the lumped parameters model of the pump. We incorporated the methods into our global model and evaluated their performance in terms of accuracy and required computational times. The results obtained and the impact on the teeth gaps geometry are finally compared and discussed.

1. Introduction

The Gerotor pump is a positive displacement pump with characteristics of simplicity, compactness, and robustness. It finds use in many sectors such as aerospace (for lubrication, cooling, and as fuel pump), automotive (for engine or transmission lubrication circuits) and more standard hydraulic applications. The Gerotor pump consists of a few elements: an inner gear, an outer gear, a valve plate, and a housing. The pump chambers are defined between the two gears and, during their meshing, the volume of the chambers increases and decreases. These chambers are connected to the suction and discharge environments through appropriate ports realized on the valve plate[1].

Since this type of pump has such wide-ranging applications, different studies exploiting the use of simulation models have been developed over the years. These models can be divided into CFD or lumped parameters models (0D fluid dynamic models)[2]. The CFD model is more complex and requires more computational time than a lumped parameters model, that can provide good results with smaller computation time. This last approach seems the most suitable when simulation is integrated in the design process for a new prototype for example. The use of virtual simulation during the design phase gives the possibility to choose the best design options to obtain the desired performance, such as flow rate or pressure ripple, while analysing at the same time the pump noise emissions, and the efficiency of the machine, an extremely important topic nowadays. Of course, the modelling of the pump can be performed using different levels of detail in terms of phenomena taken into consideration, such

as thermal effects, cavitation, deformation, or micro-movements of the mechanical parts; some examples coming from the literature are discussed below.

R. Castilla et al.[3] developed a 3D CFD models of a mini-Gerotor pump using OpenFOAM and calculated the instantaneous flow ripple. G. Altare and M. Rundo[4] developed a 3D CFD models with PumpLinx to study the influence of Gerotor geometric features on the filling capability. M. Pellegri et al.[5] compared the capability of estimated pressure and flow rate of CFD model with a 0D model, combined a 0D model with CFD to estimate the lateral leakages of a Gerotor pump and studied the influence of the lateral gaps geometry on the pump's performance[6].

M. Fabiani and al. in [7] presented a lumped parametric model to estimate the fluid dynamics performances of a Gerotor pump. Again, M.Pellegri and A.Vacca in [8] discussed the 0D model of the Gerotor, taking into account the micro-displacement of the outer gear. Z. Misty at al.[9] developed a 0D model capable to estimate the fluid dynamic and mechanical performance of a Gerotor pump. Milani et. al in [10] and [11] applied similar simulation approaches to study both Orbit and Gerotor machines.

In conclusions, there are a lot of works in literature discussing these pumps, but despite all the contributions and the apparent simplicity of the machine, there is not available a unique simulation tool that can be used in the design process with enough confidence and that analyses all the critical issues of the machine and there are no clear indications about the efficacy of simplified approaches applied to evaluate the pump performance versus more complex approach, depending on the phenomena that would be analysed. Of course, this means that mainly the expertise of the designer and an expensive experimental activity allow to complete a proper design of this kind of pumps. The activity initiated by the work of this paper would like to cover this point and to address this issue.

Specifically in this paper, we propose a lumped parametric model to estimate the dynamic and steady-state fluid dynamic performances of a Gerotor pump, considering the contribution of the main leakages through the gaps inside the pump, and proposing ways to integrate the calculation of micro-displacements of the outer gear, assuming the inner gear is fixed. The aim is to show that this aspect is playing a significant role on the pressure transients inside the pumping chambers and hence globally on the pump performance. We model the coupling outer gear-housing as a journal bearing. In section 2, we propose three different methods to study the behaviour of journal bearings under dynamic load. One of these three methods, the mobility method, is also used by M. Pellegri and A. Vacca[8]. In section 3, we compare these three methods by applying them to a simple journal bearing case to validate our numerical model. In section 4, we describe the entire lumped parameter model. In section 5, we compare the 0D model that consider the micro-displacement with a model that assumes the outer gear centre is fixed. The comparison shows the effect of micro-displacement on gap geometry and the pump performance.

2. Journal bearing models

We treated the outer gear-pump housing coupling like a journal bearing as shown in figure 1 and below. We describe and compare three different methods for modelling the journal bearing under dynamic loading.

2.1. Method 1

To study the journal bearing behaviour we used the Reynolds equation (1) for Newtonian and incompressible fluid [12], applied to the gap between the casing and the external gear.

$$\frac{1}{r_1^2}\frac{\partial}{\partial\theta}\left(h^3\frac{\partial P}{\partial\theta}\right)+\frac{\partial}{\partial z}\left(h^3\frac{\partial P}{\partial z}\right)=6\mu\omega\frac{\partial h}{\partial\theta}+12\mu\frac{\partial h}{\partial t} \qquad (1)$$

In the Gerotor case the condition $\frac{L}{D}\ll 1$, where L is the width of the gear along axial direction and D the mean diameter, is valid, so we can apply the Ocvirk or short bearing condition [13]. This condition assumes negligible the term $\frac{1}{r_1^2}\frac{\partial}{\partial\theta}\left(h^3\ \frac{\partial P}{\partial\theta}\right)\ \approx 0$ of equation (1).

$$\frac{\partial}{\partial z}\left(h^3\frac{\partial P}{\partial z}\right) = 6\mu\omega\frac{\partial h}{\partial \theta} + 12\mu\frac{\partial h}{\partial t} \quad (2)$$

The term h is the height of the gap expressed in equation (3)as function of the clearance c and eccentricity ε:

$$h(\theta, t) = c(1 - \varepsilon\cos(\theta - \Phi)) \quad (3)$$

The relative eccentricity $\varepsilon(t)$ and the attitude angle $\Phi(t)$ allow to define the position of the journal centre at the instant t respect to the reference system Oxy, as show the figure 1 .

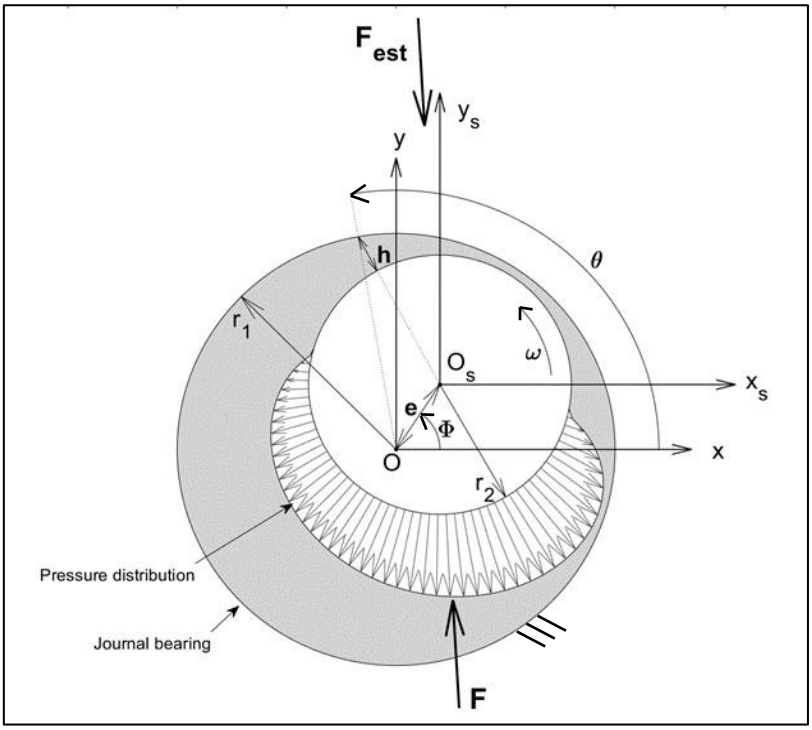

Figure 1- Journal bearing system.

By integrating the Reynolds equation (3) with the boundary conditions $P\left(\theta, z = \pm\frac{L}{2}\right) = 0$, we obtain the pressure distribution inside the gap (4) [12] .

$$p\left(\theta, z, \varepsilon(t), \Phi(t), \dot{\varepsilon}(t), \dot{\Phi}(t)\right) = \frac{3\mu}{c^2}\left(\frac{\left(\omega - 2\dot{\Phi}\right)\varepsilon\sin(\theta - \Phi)}{(1 - \varepsilon\cos(\theta - \Phi))^3} - \frac{2\,\dot{\varepsilon}\cos(\theta - \Phi)}{(1 - \varepsilon\cos(\theta - \Phi))^3}\right)\left(z^2 - \frac{L^2}{4}\right) \quad (4)$$

The hydrodynamic force (5) acting on the journal is calculated by numerically integrating the pressure distribution on the surface of the journal, considering only the terms of positive pressure assuming that the pressure is equal to the vapour pressure value for the fluid in the section where the numerical result would be negative [12].

$$\begin{pmatrix} F_x(\varepsilon(t), \Phi(t), \dot{\varepsilon}(t), \dot{\Phi}\,(t)) \\ F_y(\varepsilon(t), \Phi(t), \dot{\varepsilon}(t), \dot{\Phi}\,(t)) \end{pmatrix} = -\int_{-\frac{L}{2}}^{\frac{L}{2}}\int_0^{2\pi} p(\theta, z)\begin{pmatrix}\cos(\theta)\\ \sin(\theta)\end{pmatrix} d\theta\, dz \quad (5)$$

Knowing the external load on the journal $\boldsymbol{F_{est}}$ at time instant t, the resolution of the motion equation (6) gives the position of journal centre.

$$\begin{pmatrix} F_{estx} \\ F_{esty} \end{pmatrix} = \begin{pmatrix} F_x(\varepsilon(t), \Phi(t), \dot{\varepsilon(t)}, \dot{\Phi}(t)) \\ F_y(\varepsilon(t), \Phi(t), \dot{\varepsilon(t)}, \dot{\Phi}(t)) \end{pmatrix} \quad (6)$$

2.2. Mobility method

The mobility method (MM) is a method for analysing the behaviour of a journal bearing subjected to a dynamic load, developed by J. Booker [14] [15] [16]. This method can be applied for different values of the L/D ratio, but in this paper only the case of short bearing is considered. The position of the centre of the journal relative to an observer integral with the load can be found by solving the following system of explicit equations [17] [18]:

$$\dot{\varepsilon} = \frac{F_{est}\left(\frac{c}{R}\right)^2}{\mu\, L\, D} M^{\varepsilon}(\varepsilon, \Phi, \frac{L}{D}) \quad (7)$$

$$\dot{\Phi} = \frac{F_{est}\left(\frac{c}{R}\right)^2}{\mu\, L\, D\varepsilon} M^{\Phi}\left(\varepsilon, \Phi, \frac{L}{D}\right) + \bar{\omega} \quad (8)$$

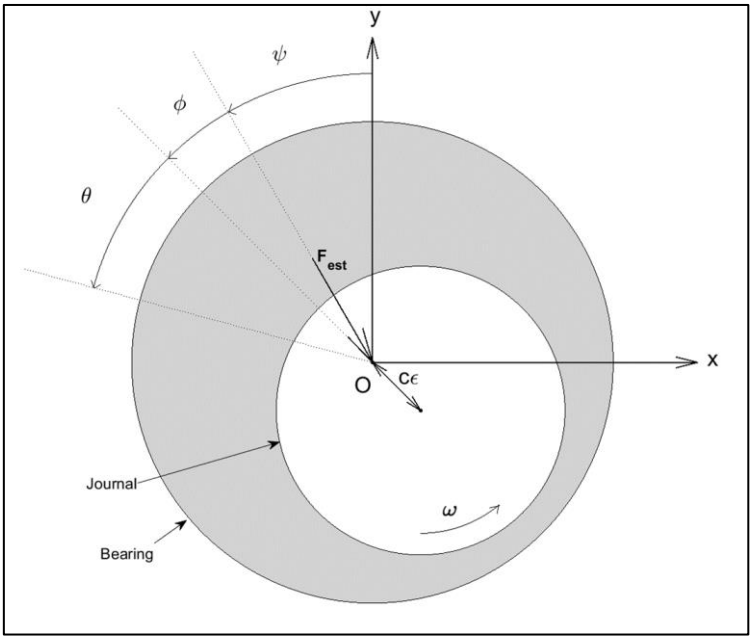

Figure 2 - Journal bearing system for mobility method.

With

$$\begin{cases} M^{\zeta} = \dfrac{(1-\zeta)^{\frac{5}{2}}}{\pi\left(\frac{L}{D}\right)^2} \\ M^{\kappa} = -\dfrac{4\kappa(1-\zeta)^{\frac{1}{2}}}{\pi\left(\frac{L}{D}\right)^2} \end{cases} if\ F_{est} \geq 0 \quad \begin{cases} M^{\zeta} = \dfrac{(1+\zeta)^{\frac{5}{2}}}{\pi\left(\frac{L}{D}\right)^2} \\ M^{\kappa} = \dfrac{4\kappa(1+\zeta)^{\frac{1}{2}}}{\pi\left(\frac{L}{D}\right)^2} \end{cases} if\ F_{est} < 0 \quad (9)$$

Where:

$$M^{\varepsilon} = M^{\zeta} cos\Phi + M^{\kappa} sin\Phi \quad (10)$$

$$M^{\Phi} = -M^{\zeta} sin\Phi + M^{\kappa} cos\Phi \quad (11)$$
$$\zeta = \varepsilon \, cos\Phi \quad (12)$$
$$\kappa = \varepsilon \, sin\Phi \quad (13)$$

2.3. Finite difference methods

We consider the rectangular domain obtained by unwrapping the journal bearing (figure 3) and rewriting the Reynolds equation (1) in this domain introducing the change of variable $x = \theta \, r_1$, we obtain [19]:

$$\frac{\partial}{\partial x}\left(h^3 \frac{\partial p}{\partial x}\right) + \frac{\partial}{\partial y}\left(h^3 \frac{\partial p}{\partial y}\right) = 6 \, \mu \, \omega \, r_2 \frac{\partial h}{\partial x} + 12 \, \mu \frac{\partial h}{\partial t} \quad (14)$$

The gap height is expressed as:

$$h(x,t) = c - e_x(t) \cos\left(\frac{x}{r_1}\right) - e_y(t) \sin\left(\frac{x}{r_1}\right) \quad (15)$$

With $\boldsymbol{e} = \left(e_x, e_y\right)$ eccentricity vector.

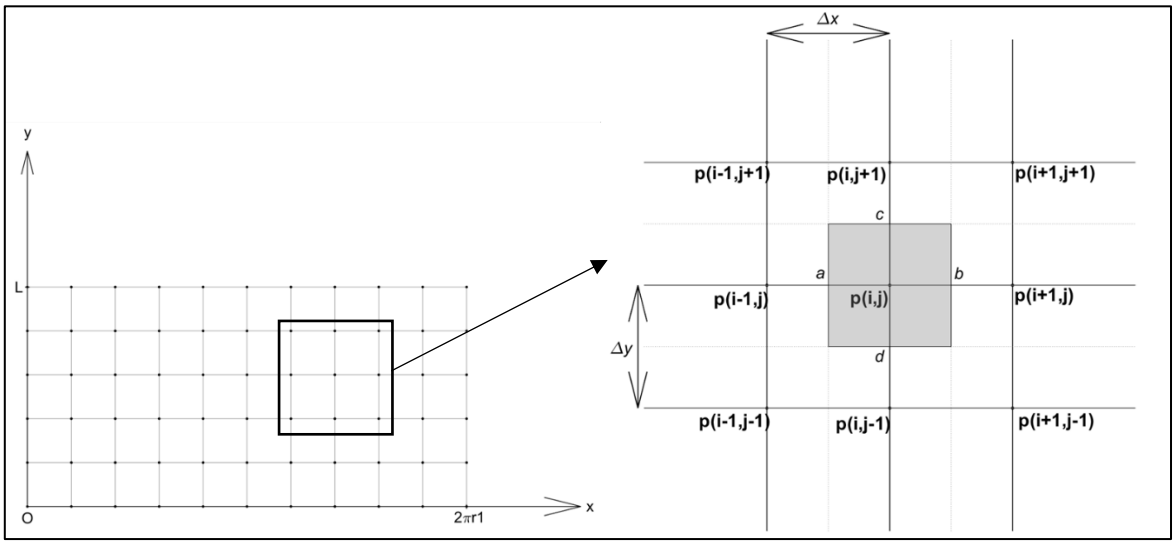

Figure 3 - Unwrapped fluid film in the film Cartesian reference system.

The rectangular domain is discretized in a finite number of points $N_x * N_y$, while the terms of Reynolds equation (14) are discretized in the following ways [20]:

- $\frac{\partial}{\partial x}\left(h^3 \frac{\partial p}{\partial x}\right) \approx \frac{\left(h^3 \frac{\partial p}{\partial x}\right)|_b - \left(h^3 \frac{\partial p}{\partial x}\right)|_a}{\Delta x}$
- $\left(\frac{\partial p}{\partial x}\right)|_b = \frac{p(i+1,j) - p(i,j)}{\Delta x} \qquad (h^3)|_b = h_b^3 = \left(\frac{h(i+1,j) + h(i,j)}{2}\right)^3$
- $\left(\frac{\partial p}{\partial x}\right)|_a = \frac{p(i,j) - p(i-1,j)}{\Delta x} \qquad (h^3)|_a = h_a^3 = \left(\frac{h(i,j) + h(i-1,j)}{2}\right)^3$
- $\frac{\partial}{\partial y}\left(h^3 \frac{\partial p}{\partial y}\right) = h^3 \frac{\partial^2 p}{\partial y^2} \approx h(i,j)^3 \frac{\left(\frac{\partial p}{\partial y}\right)|_c - \left(\frac{\partial p}{\partial y}\right)|_d}{\Delta y}$
- $\left(\frac{\partial p}{\partial x}\right)|_c = \frac{p(i,j+1) - p(i,j)}{\Delta x} \qquad \left(\frac{\partial p}{\partial x}\right)|_d = \frac{p(i,j) - p(i,j-1)}{\Delta x}$
- $\frac{\partial h}{\partial x} \approx \frac{h(i+1,j) - h(i-1,j)}{2 \, \Delta x}$

- $\frac{\partial h}{\partial t} \approx -\frac{e_x(t)-e_x(t-\Delta t)}{\Delta t}\cos\left(\frac{x_i}{r_1}\right) - \frac{e_y(t)-e_y(t-\Delta t)}{\Delta t}\sin\left(\frac{x_i}{r_1}\right)$

From the discretization of the Reynolds equation for each point of the domain we obtain a system of linear equations:

$$\bar{\bar{C}}\,\boldsymbol{p} = \boldsymbol{s} \qquad (16)$$

Where:

- $\bar{\bar{C}}\left(e_x(t), e_y(t)\right)$ is the coefficient matrix of $\left(N_x * N_y\right)^2$ elements [m].
- $\boldsymbol{p}$ is the vector of unknowns of $\left(N_x * N_y\right)$ elements [Pa].
- $\boldsymbol{s}(e_x(t), e_y(t))$ is the vector of knowns of $\left(N_x * N_y\right)$ elements [Pa m].

The resolution of system (16) gives the pressure distribution inside the gap. The pressure distribution is used to calculate the hydrodynamic force on journal, but only the positive values of $p(i,j)$ are considered, neglecting the negative values to consider the effect of cavitation[12].

$$F_x(e_x(t), e_y(t)) = -\sum p(i,j)\,\Delta x\,\Delta y \cos\left(\frac{x_i}{r_1}\right) \qquad (17)$$

$$F_y(e_x(t), e_y(t)) = -\sum p(i,j)\,\Delta x\,\Delta y\, sin\left(\frac{x_i}{r_1}\right) \qquad (18)$$

Knowing the external load on the journal $\boldsymbol{F_{est}}$ at time instant t, the resolution of the motion equation (19) gives the position of journal centre.

$$\begin{pmatrix} F_{estx} \\ F_{esty} \end{pmatrix} = \begin{pmatrix} F_x(e_x(t), e_y(t)) \\ F_y(e_x(t), e_y(t)) \end{pmatrix} \qquad (19)$$

2.4. Method comparison

Here in the following, we compare the trajectory obtained applying the three methods to a journal bearing under dynamic load. The geometry of the journal bearing and the operating conditions are shown in the table 1, while the loading is shown in the figure 4.

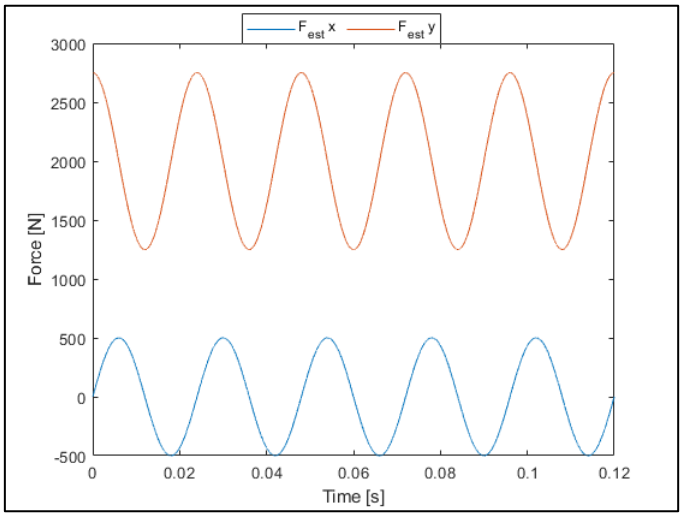

Figure 4 - The bearing load.

Method 1 and the Mobility Method calculate trajectories of the external gear centre that are similar, because both methods are based on the hypothesis of short bearing and consider only the positive pressure contributions for the calculation of the hydrodynamic forces. The FDM-based method does not

neglect any term of the Reynolds equation (14) and this leads to a different pressure distribution in the gap with respect to the other two methods, and therefore to different hydrodynamic forces.

Table 1- List of parameters used for the resolution of the journal bearing problem.

Journal bearing length L	17.2 mm	Angular velocity	500 rpm
Journal bearing diameter D	101.55 mm	Initial eccentricity ε_x	0.0997
Radial clearance c	0.0975 mm	Initial eccentricity ε_y	0.0071
Fluid viscosity μ	0.0391 Pa s		

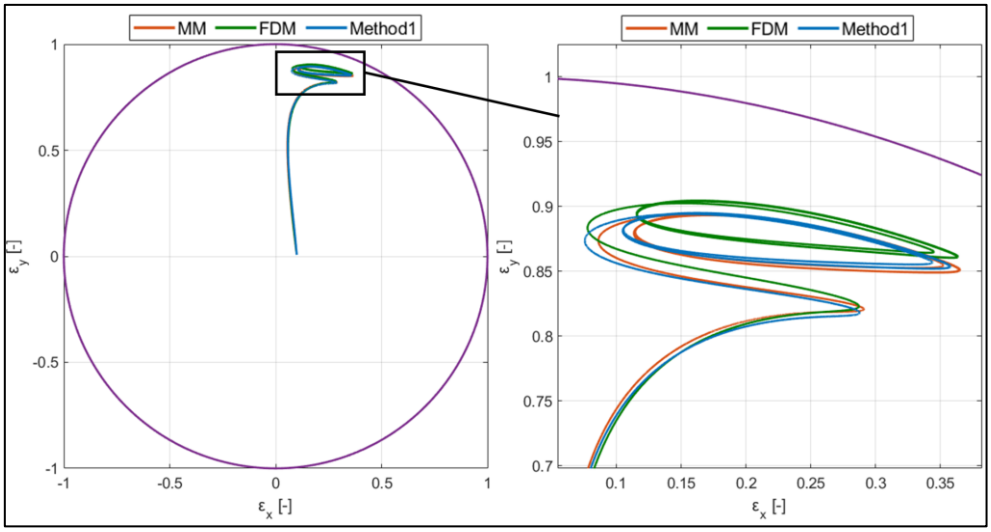

Figure 5 - Journal centre trajectory.

The FDM require more computational time that other methods. The method of least effort is the MM because one must solve only the system of differential equations (7) (8). The Method 1 require slightly more time that MM because it is necessary to solve first the linear system of equations (16) to find the hydrodynamic force (17)(18), and after the motion equation (19). In any case, given the similarity of the results, we can conclude that all the three methods can be used within the general model of the pump and hence the choice will be guided by the computational time aspect.

Table 2-Computation time of the journal bearing problem with time step of 0.0001 sec.

Mobility method	Method 1	FDM with $N_x = 320, N_y = 40$
$\sim 7\ sec$	$\sim 129\ sec$	$\sim 43560\ sec$

3. Lumped parameter model

We have developed a lumped parameter model of a Gerotor pump in MATLAB, under hypothesis of Newtonian fluid, constant density, isothermal condition, and constant operating conditions (rotational speed and low and high pressure at the ports).

In a lumped parameter model the fluid domain is divided into control volumes, enclosed between the teeth of the internal and external gears. The pressure inside the control volumes depends on the time or shaft angular position (constant angular velocity of the gears). The number of control volumes is N+2, where N is the number of chambers, and the other two control volumes are the suction and delivery ambient. The pressure inside the control volumes and the flow rate exchanged between the control volumes are calculated with the continuity equation (20) [2].

$$\frac{\mathrm{d}p}{\mathrm{d}\theta} = \frac{\beta}{V\omega}\left(\sum \mathrm{Q}_{int/out} - \frac{dV}{d\theta}\frac{1}{\omega_{int}}\right) \qquad (20)$$

The pump chambers exchange flow with contiguous chambers and suction/delivery ports.
While the suction/delivery ports exchange flow rate also between them and the drain.

The flow rate between the pump chambers and suction/delivery ports is modelled using the turbulent orifice equation (21) with discharge coefficient (C_d) that depends on the Reynolds number [8] [21].

$$Q = sign(\Delta p)\, C_d\, A \sqrt{\frac{2|\Delta p|}{\rho}} \qquad (21)$$

The adjacent chambers communicate with each other through the gaps between the tips of the teeth of the two gears and the lateral gaps between the gears and the pump housing.

3.1. Leakage across teeth tips

The clearances between the teeth tips of inner and outer gears are defined according to the manufacturing tolerances [22] [7].

Under laminar flow hypothesis, the leakages across the teeth tips between the contiguous chambers are modelled with the Poiseuille equation, with the addition of the Couette flow term. For the generic chamber *j*, the equation is (22) [8] [5].

$$sign(p_{j-1} - p_j)\frac{b\, {h_{j-1}}^3}{12\,\mu}\frac{|p_{j-1} - p_j|}{le_{j-1}} + sign(p_{j+1} - p_j)\frac{b\, {h_j}^3}{12\,\mu}\frac{|p_{j+1} - p_j|}{le_j} + \frac{v_{r\,j-1}}{2}\, b\, h_{j-1} - \frac{v_{r\,j}}{2}\, b\, h_j \qquad (22)$$

The control volume *j* is bounded by the gaps formed by the inner gear with the *j* and *j-1* teeth of the outer gear. The terms h_{j-1} and h_j are the minimum heights of *j* and *j-1* gaps. The equivalent lengths of gaps, le_{j-1} and le_j, are defined as the distance between the points of gap where the gap height is $h^* = h(1 + dh)$ [8] [5].

While the terms $v_{r\,j-1}$ and $v_{r\,j}$ are the relative speeds between the inner /outer gears at the point of minimum height gap.

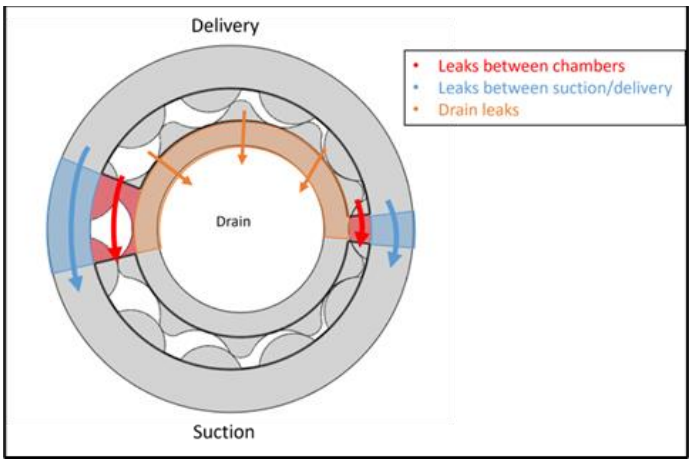

Figure 6- Geometry of lateral gaps.

3.2. Lateral leakage

The lateral gaps are formed by the wheels face and pump housing along axial direction. The lateral leakages between contiguous chambers happen near the start/end suction and delivery ports, figure 6.

We modelled these leakages with the method proposed by P. J. Gamez-Montero and E. Codina [23,24].This method uses of the Poiseuille and Couette terms to express the leakages.

3.3. Leakage between suction and delivery

We assume that suction and delivery ambient are connected across the lateral gaps formed by outer wheel and pump housing, highlight in figure 6. We use the Poiseuille formula to describe the flow from delivery to suction control volume[22].

3.4. Drain leakage

We assume that the drain pressure is the same of the suction ambient, so there is only flow rate from delivery control volume to drain across the later gap formed by the inner wheel and pump housing, as highlighted in figure 6. We use the Poiseuille formula to describe the drain leakage [22].

3.5. Fluid model

The fluid model takes into account the cavitation occurrence in a very simplified way. This model acts only on the fluid bulk modulus while the other fluid properties remain constant. The bulk modulus is equal to β^* for positive relative pressure values, while for negative relative pressure values the bulk modulus is reduced by three orders of magnitude.

$$\beta(p) = \begin{cases} \beta^*, & p \geq 0 \\ \beta^*/1000, & p < 0 \end{cases} \quad (23)$$

3.6. Micro-displacement outer gear

The calculate of the external force acting on the outer gear, it is necessary to define the radial micro-displacement of outer gear.

The external force applied to the outer gear is the sum of the fluid pressure force and the contact force between the two gears.

The pressure force acting on the outer gear due to the pressure inside the generic chamber j can be calculated as [8] [5]:

$$\boldsymbol{F_{pj}} = p_i \, l_{y_j} \, L \, \boldsymbol{i} + p_j \, l_{x_j} \, L \, \boldsymbol{j} \quad (24)$$

The terms $l_{x_j}$and l_{y_j} are the projections of the area chamber j along the x and y axis, as show in figure 7.a. The torque contribution of the pressure forces of chamber j can be calculated as:

$$\boldsymbol{C_{pj}} = \left(p_j \, l_{y_j} \, b_{y_j} + p_j l_{x_j} \, b_{x_j}\right) L \, \boldsymbol{k} \quad (25)$$

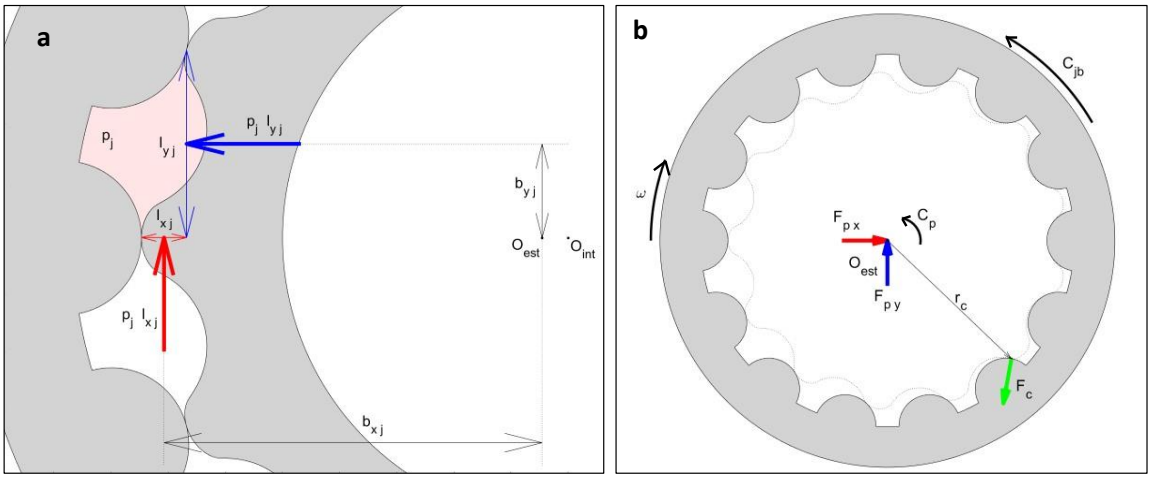

Figure 7- **a**: Pressure force component and arm for one chamber;
b: Free body diagrams for the outer rotor.

The terms b_{x_j} and b_{y_j} are the arms of the pressure force respect to the center of the outer gear.
Defining the total torque due to of the contributions of the individual chambers as **Cp** and assuming a single point of contact between the gears, the contact force **Fc** can be found by solving the following rotational equilibrium.

$$\boldsymbol{C_p + C_{jb} + r_c \times F_c = 0} \quad (26)$$

The term $\boldsymbol{C_{jb}}$ represents the viscous friction torque on the surface of the outer gear, which we approximate as [12]:

$$\boldsymbol{C_{jb}} = \frac{\mu\, \omega_{est}\, L\, r_1^2}{c} \frac{2\,\pi}{(1-\varepsilon^2)^{1/2}}\ \boldsymbol{k} \quad (27)$$

Finally, the load acting on the outer gear must be balanced by the fluid dynamic forces $\boldsymbol{F_{est} = F_p + F_c}$.

3.7. Gears overlap check

The journal bearing models do not consider the presence of the inner gear and the consequent possible overlapping between the gears. To avoid overlap and to calculate the height of the teeth tips gaps, we have proceeded as described in the following.

We assumed that the centre of the inner gear is fixed. We calculated the displacement vector of the outer gear centre with respect to its nominal position, $\mathbf{e} = (e_x, e_y)$, using one of three journal bearing models.

The gears centres are placed in their nominal positions, with the inner gear in the angular position θ and the outer gear in the angular position $\theta \frac{N-1}{N}$, as show in figure 8, In the figure 8 the clearances between inner and outer gear are increased for a better visualization.

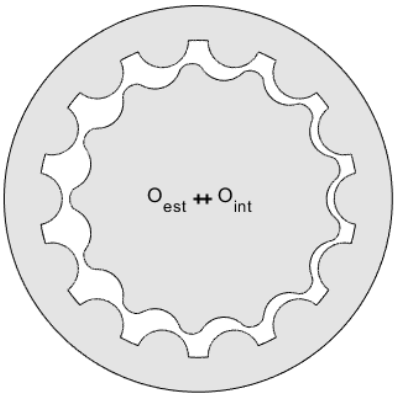

Figure 8- Initial condition overlap check

The outer gear centre is moved of (e_x, e_y) from nominal position O_{est} to new position O'_{est} and the gears overlap is checked, figure 9.a and figure 10.a.

- *If there is overlap* (figure 9): the outer gear is moved along the direction of vector (e_x, e_y) just enough to have only one point of contact between gears and no overlap. As show in figure 9.b, the centre of outer gear is moved of ΔS from O'_{est} to O^*_{est}. In this way there is one contact point and there isn't overlap. ΔS is the max overlap between the two gears along the direction of vector $\boldsymbol{e}$ and it is calculated automatically inside the model. Once the correct position of the outer gear is found, the heights of the teeth tips gaps are calculated.
- *If there is not overlap* (figure 10)*:* in this case after the translation of the outer gear from O_{est} to O'_{est}, there aren't contact points between the gears (figure 10.a). So, the inner gear is rotated by small angular steps automatically by the model until the two gears are in contact in one point (figure 10.b) and the heights of the teeth tips gaps are then calculated.

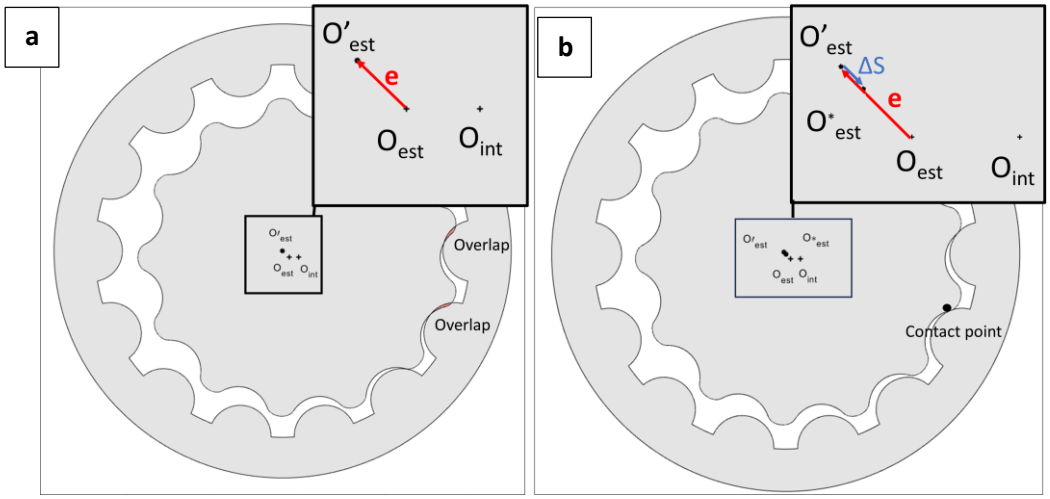

Figure 9 - **a**: Overlap condition . **b:** Outer gear translation of ΔS to avoid the overlap

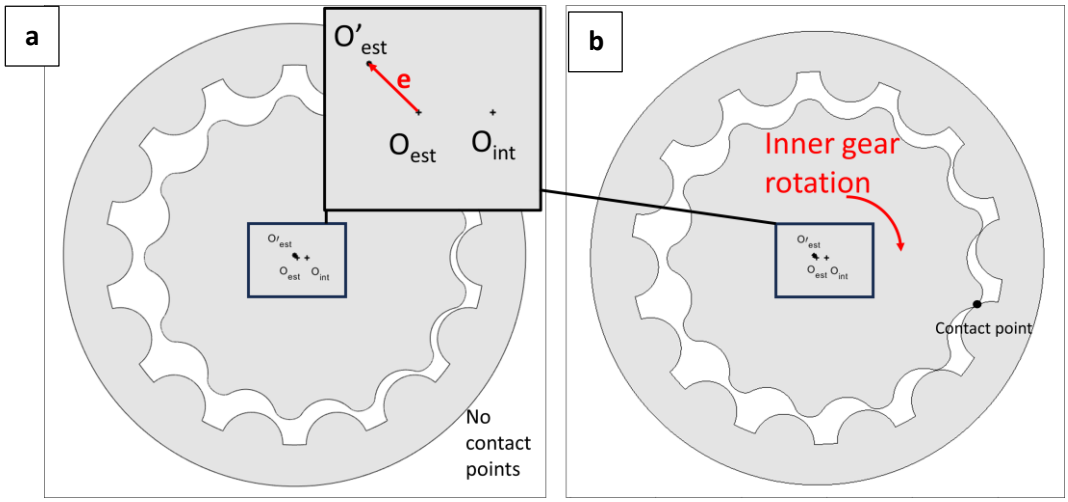

Figure 10 - **a**: No overlap condition . **b:** Inner gear rotation to have one contact point

4. Lumped parametric models results

In this paragraph we have made the comparison between the lumped parameter models obtained by applying the three journal bearing models of section 2, with the addition of another model in which we have considered fixed the outer gear, with the gear centre in its nominal position. Due to the simple fluid model used, we made the comparison by imposing a low rotational speed and high discharge pressure in order to avoid excessive cavitation phenomena and unrealistic sub-zero relative pressure values. The delivery load was obtained by inserting a restriction on the delivery line with the same diameter for all models.

The pump analysed can operate in the range 0-3000 rpm and 0-27.5 bar.

The comparison of the trajectories of the gear centre, tooth head heights and pressures are shown in the figure 13, 14, 15 and 16. It is noted that the three models with micro-displacements of the outer gear give very similar results; then, we focus on comparing the three models with the micro-displacement calculation with the case of external gear with fixed centre.

Figure 14 shows the pressure trend inside a pump chamber as a function of the inner gear position. The reference chamber analysed is highlighted in figure 11 where it is called Chamber 1. In the position shown in figure 11 the reference angular position of the inner gear is equal to zero.
As we can see in figure 14:

- the models with micro-displacement have a pressure trend like the model with fixed gear during the suction phase;
- the models with micro-displacement have a different pressure trend to the model with fixed gear during the delivery phase;
- the model with fixed gear has more pronounced depression phenomenon than the models with micro-displacement near the transition from delivery to suction.

The pressure in models with micro-displacements is on average higher than in the model with fixed gear, as shown in figure 15

These differences can be explained by looking at the figure 16.a and 16.b, which show the height and equivalent length of a tooth head gap (tooth 1 of figure 11) as a function of the angular position of the inner gear.
The micro-displacements of the outer gear influence the geometry of the teeth head gaps and consequently also the pressure and leakages values compared to the case with fixed external gear, while we assumed the geometry of lateral gaps is independent from the micro-displacement. In the case considered, the pressure in the delivery phase of the chamber models with micro-displacements is higher because the chamber has lower leaks through the teeth head gaps than in the case with fixed gear. In the transition from delivery to suction the chamber of the model with fixed gear is characterised by smaller leaks and this causes a stronger depression. This demonstrates the influence of the micro-displacement on model results.

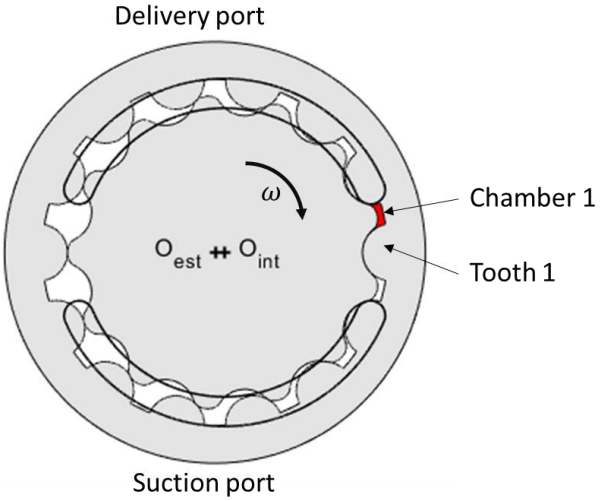

Figure 11- Chamber one with the inner gear in zero angular position

Other aspects emerged from the models are:

- At a constant angular velocity, increasing the delivery pressure causes the trajectory of the outer gear centre to move to the left (see the reference system of figure 13);
- While at a constant delivery pressure, increasing the angular velocity causes the trajectory of the outer gear centre to move to the right (see the reference system of figure 13).

So, the operating condition affects the shape and position of the trajectory of the outer gear centre, as well as the geometry of the teeth gaps. In the model with the outer gear fixed centre, the gaps' geometry is independent from the operating condition. The figure 12 shows the effect of pressure and angular velocity on the height of the tooth gap (the data is obtained using the mobility method 0D

model). In the case of high speed, the effect of pressure increase is more pronounced than in the low-speed case.

Since the three models produce very similar results, a factor to choosing one of the three models is the calculation time. The micro-displacement model using the mobility method is preferable because it requires less calculation time.

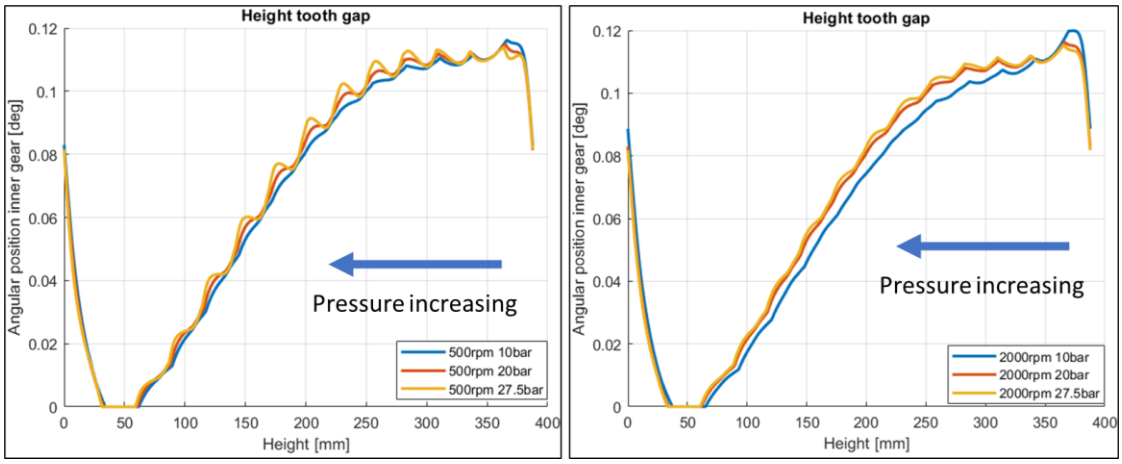

Figure 12- Height tooth gap MM model at different pressure and velocity

The tables 3, 4 and *5* presents a comparison between the volumetric efficiencies estimated by two models: one with a fixed outer centre gear and the other based on the mobility method. The micro-motion model estimates a higher volumetric efficiency compared to the case of the fixed outer gear centre.

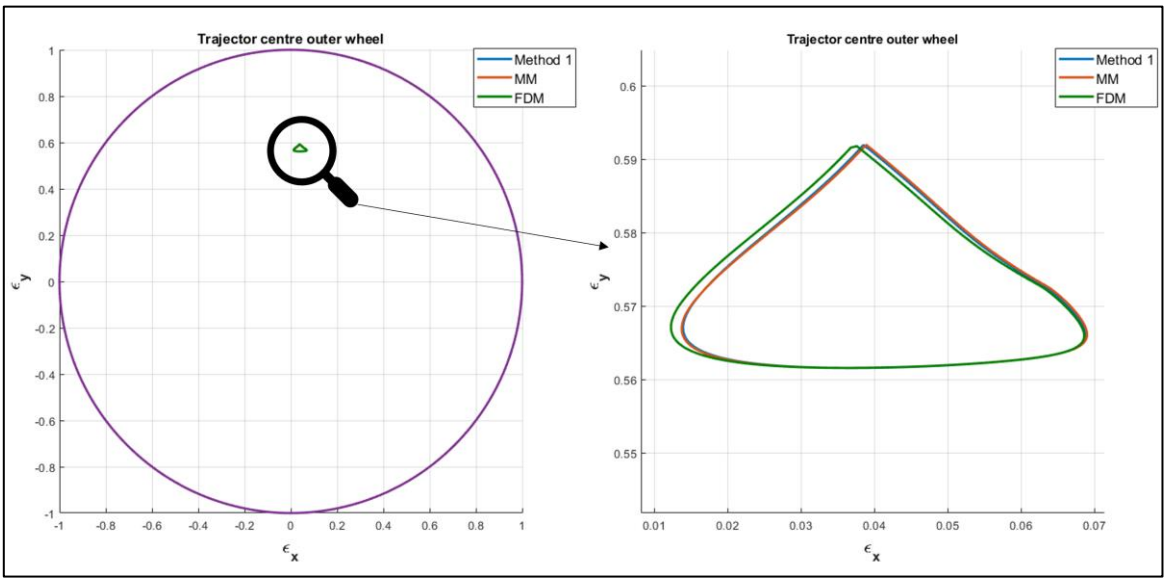

Figure 13 Comparison trajectory centre of outer gear.

Table 3- Volumetric efficiency at 1000 rpm

	5 bar	10 bar	15 bar	20 bar	25 bar	27.5 bar
Fix centre	91.97 %	85.77 %	79.56 %	73.35 %	67.15 %	64.04 %
MM	93.32 %	87.24 %	81.16 %	75.08 %	69.00 %	65.96 %

Table 4 - Volumetric efficiency at 2000 rpm

	5 bar	10 bar	15 bar	20 bar	25 bar	27.5 bar
Fix centre	95.04 %	91.15 %	88.86 %	85.78 %	82.69 %	81.15 %
MM	96.73 %	93.73 %	90.73 %	87.73 %	84.73 %	83.23 %

Table 5 - Volumetric efficiency at 3000 rpm

	5 bar	10 bar	15 bar	20 bar	25 bar	27.5 bar
Fix centre	96.14 %	94.06 %	91.99 %	89.91 %	87.83 %	86.79 %
MM	97.62 %	95.67 %	93.71 %	91.75 %	89.79 %	88.81 %

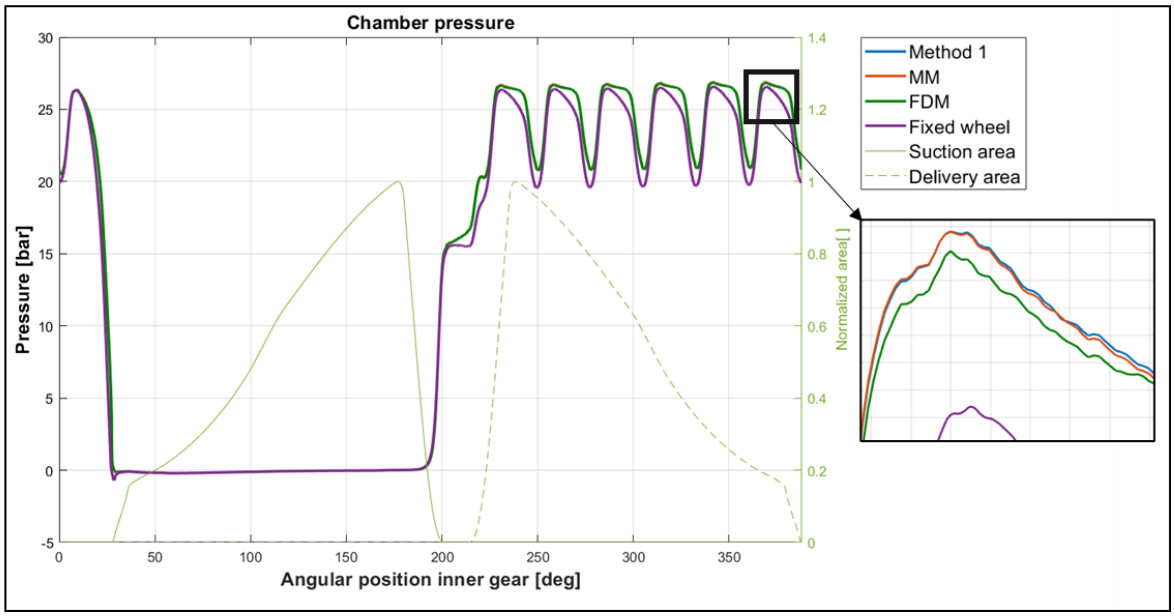

Figure 14 – Pressure inside a single chamber of pump.

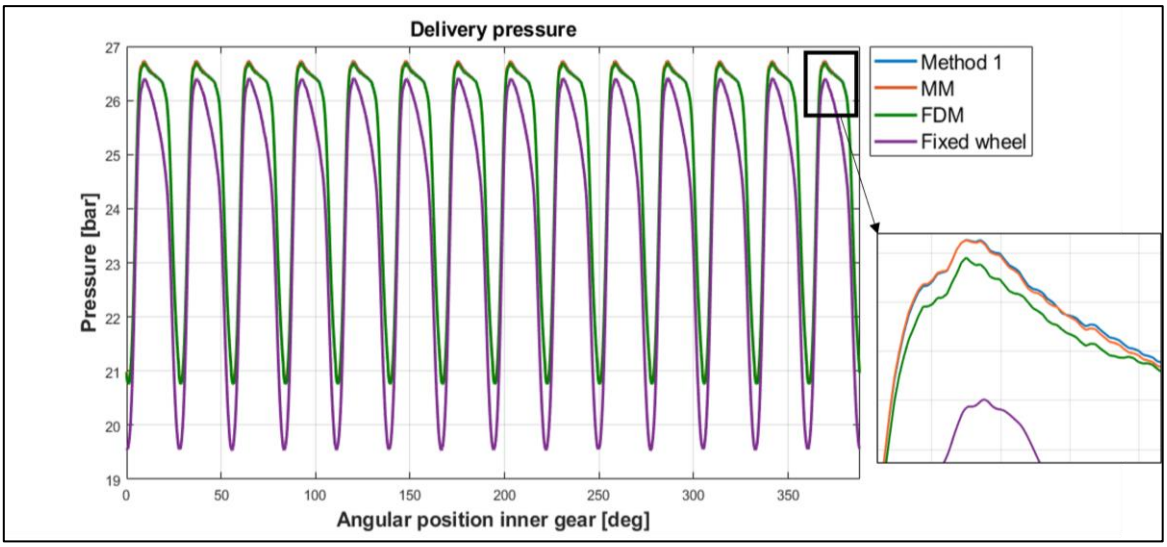

Figure 15- Delivery pressure.

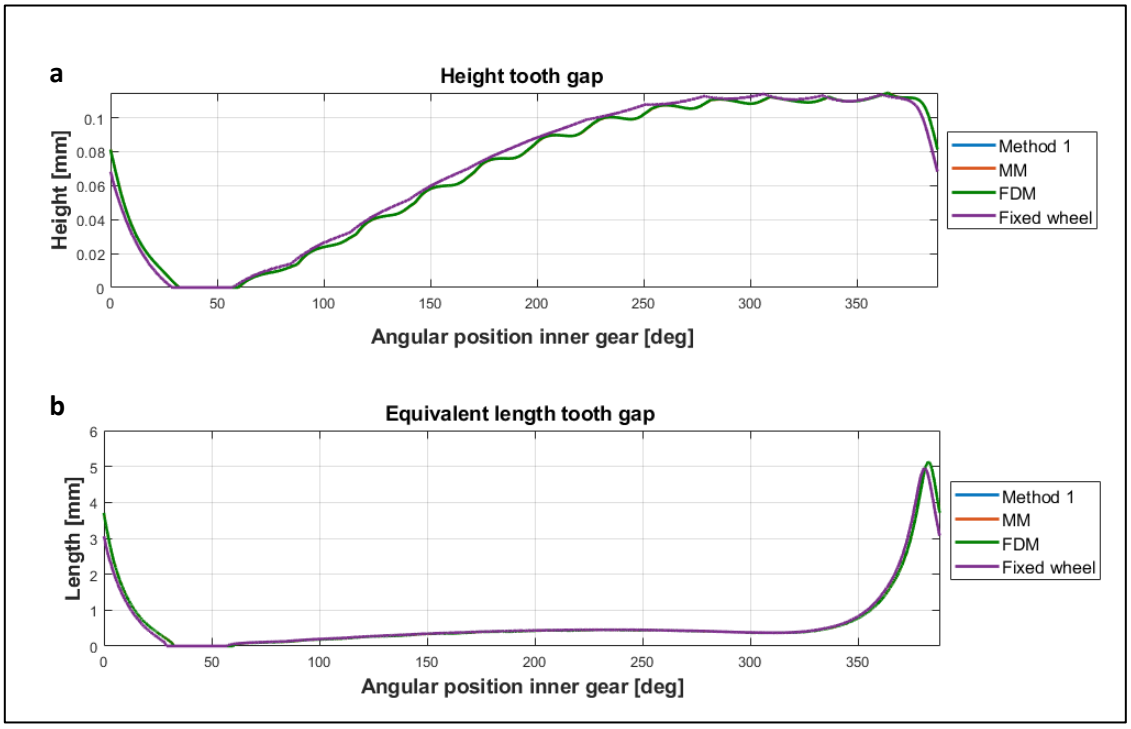

Figure 16– **a**: Height tooth gap; **b**: Equivalent length of tooth gap.

5. Conclusion

In this paper we have introduced three different methods to study the behaviours of the external gear inside the casing of a Gerotor pump under dynamic load. We have presented three methods to modelling the micro-displacement of the outer gear integrated later in the lumped parameter fluid-dynamic model of the pump. The three models give very similar results, so we have confronted the micro-displacement model with a model that consider the outer gear fixed in their nominal position. The comparison showed that the micro-displacement of outer gear influences the geometry of teeth head gaps and consequently the pressure and flow rate model output. Because it requires less time calculation, we consider the mobility method more suitable to be integrated inside a lumped parametric model.

The next activities of the research project will be:

- insert a more complex fluid model in order to describe better the cavitation;
- validate the pressure prevision of the model with experimental test or CFD analysis.

6. Nomenclature

A orifice area [m^2]

b axial length gears [m]

b_x b_y pressure force arms [m]

b_d width lateral gap between drain/delivery port [m]

$b_{int}(\theta)$, $b_{est}(\theta)$ the width of the lateral gap between the inner/outer gear and the pump housing (Couette flow) [m]

$c = r_2 - r_1$ radial clearance [m]

$\boldsymbol{C_d}$ discharge coefficient [-]

$\boldsymbol{C_{jb}}$ viscous friction torque outer gear [N m]

r_1 r_2 radii of bearing and journal [m]

$\boldsymbol{r_c}$ contact force arm [m]

re_int min radius of lateral gap of outer gear with respect O_{est} [m]

ri_est max radius of lateral gap of inner gear with respect O_{int} [m]

ri_inf root radius inner gear [m]

t time[s]

$\boldsymbol{C_p}$ pressure torque outer gear [N m]

$D = 2r_2$ bearing diameter [m]

$\boldsymbol{e} = (e_x, e_y)$ eccentricity [m]

$\boldsymbol{F} = (F_x, F_y)$ hydrodynamic force [N]

F_c contact force [N]

$\boldsymbol{F_{est}} = (F_{est\,x}, F_{est\,y})$ journal bearing external load [N]

$\boldsymbol{F_p}$ pressure force outer gear [N]

G external radius of outer gear [m]

h height gap [m]

L journal bearing axial length [m]

L_d length lateral gap between drain/delivery port [m]

le equivalent length gap [m]

l_x l_y volume chamber projection along x e y axis [m]

$\boldsymbol{M} = (M^{\varepsilon}, M^{\Phi})$ mobility vector [-]

p pressure [Pa]

Q flow rate [m^3/s]

Re root radius outer gear [m]

Ri hole radius inner gear [m]

N number of pump chambers [-]

N_x N_y number of mesh points in $\hat{x}$ and $\hat{y}$ direction [-]

$O\ x\ y\ z$ reference system for the bearing [-]

$O_s\ x_s\ y_s\ z_s$ reference system for the journal [-]

$\hat{O}\ \hat{x}\ \hat{y}$ reference system for the unwrapped film [-]

$\bar{\omega} = \frac{\omega}{2} - \dot{\psi}$ average angular velocity of journal relative external load F_{est} [rad/s]

$\overline{v_{int}}(\theta)$ e $\overline{v_{est}}(\theta)$ the relative speed between the inner/outer gear and the pump housing at the midpoint of the lateral gap (Couette flow) [m/s]

v_r relative velocity [m/s]

z journal bearing axial position [m]

β fluid bulk modulus [Pa]

$\Delta x\ \Delta y$ mesh length [m]

Δp pressure drop across the orifice [Pa]

Δt time step [s]

$\varepsilon = |e|/c$ relative eccentricity [-]

$\dot{\varepsilon} = \frac{d\varepsilon}{dt}$ [1/s]

θ journal bearing angular position [rad]

μ fluid dynamic viscosity [Pa s]

ρ fluid density [kg/m^2]

Φ attitude angle [rad]

$\dot{\Phi} = \frac{d\Phi}{dt}$ [rad/s]

χ_1 , χ_2 angular extension lateral gap between suction/delivery ports with respect O_{est}[rad]

χ_3 angular extension lateral gap between drain/delivery port ports with respect O_{int} [rad]

$\dot{\psi}$ angular velocity of external load F_{est} [rad/s]

ω angular velocity of journal [rad/s]

ω_{int} ω_{est} rotation speed of inner and outer gear [rad/s]

7. References

[1] Gamez-Montero P J, Codina E and Castilla R 2019 A Review of Gerotor Technology in Hydraulic Machines *Energies* **12** 2423

[2] Rundo M 2017 Models for Flow Rate Simulation in Gear Pumps: A Review *Energies* **10** 1261

[3] Castilla R, Gamez-Montero P J, Raush G and Codina E 2018 Three Dimensional Simulation of Gerotor with Deforming Mesh by using OpenFOAM *Proc. 11th Int. Fluid Power Conf.* Aachen, Germany.

[4] Altare G and Rundo M 2016 Computational Fluid Dynamics Analysis of Gerotor Lubricating Pumps at High-Speed: Geometric Features Influencing the Filling Capability *J. Fluids Eng.* **138** 111101.

[5] Pellegri M, Vacca A, Frosina E, Buono D and Senatore A 2017 Numerical analysis and experimental validation of Gerotor pumps: A comparison between a lumped parameter and a

computational fluid dynamics-based approach *Proc. Inst. Mech. Eng. Part C J. Mech. Eng. Sci.* **231** 4413–30.
[6] Pellegri M and Vacca A 2019 A Simulation Approach for the Evaluation of Power Losses in the Axial Gap of Gerotor Units *JFPS Int. J. Fluid Power Syst.* **11** 55–62.
[7] Fabiani M, Mancò S, Nervegna N, Rundo M, Armenio G, Pachetti C and Trichilo R 1999 Modelling and Simulation of Gerotor Gearing in Lubricating Oil Pumps *Int. Congress & Exposition* pp 1999-01–0626.
[8] Pellegri M and Vacca A 2017 Numerical simulation of Gerotor pumps considering rotor micro-motions *Meccanica* **52** 1851–70.
[9] Mistry Z, Manne V H B, Vacca A, Dautry E and Petzold M 2020 A numerical model for the evaluation of gerotor torque considering multiple contact points and fluid-structure interactions *12th Int. Fluid Power Conf.* Dresden, Germany.
[10] Milani M, Montorsi L, Terzi S, Storchi G and Lucchi A 2019 Analysis of a Double Inlet Gerotor Pump: A Dynamic Multi-Phase CFD Approach Accounting for the Fluid Compressibility and Temperature Dependent Properties *IMECE2019*.
[11] Babbone R, Bottazzi D, Cagni G, Grasselli F and Milani M 2011 CAE design of orbit annular machines *12th Scandinavian Int. Conf. on Fluid Power* Tampere, Finland.
[12] Ghosh M K, Majumdar B C and Sarangi M 2014 *Fundamentals of Fluid Film Lubrication* (New York: McGraw-Hill Education).
[13] Ocvirk F W 1952 Short-Bearing Approximation for Full Journal Bearings *NACA Technical Notes 2808:28.*
[14] Booker J F 1965 Dynamically Loaded Journal Bearings: Mobility Method of Solution *J. Basic Eng.* **87** 537–46.
[15] Booker J F 1971 Dynamically-Loaded Journal Bearings: Numerical Application of the Mobility Method *J. Lubr. Technol.* **93** 168–74.
[16] Booker J F 2014 Mobility/Impedance Methods: A Guide for Application *J. Tribol.* **136** 024501
[17] Flores P, Claro J P and Ambrósio J 2006 Journal bearings subjected to dynamic loads: the analytical mobility method *Mecanica Experimental*, **13**, 115-127.
[18] He T, Lu X and Zhu J 2013 Mobility Method Applied to Calculate the Lubrication Properties of Bearing under Dynamic Loads *ISRN Mech. Eng.* **2013** 1–5
[19] Du R, Chen Y and Zhou H 2018 Numerical analysis of the lubricating gap between the gear shaft and the journal bearing in water hydraulic internal gear pumps *Proc. Inst. Mech. Eng. Part C J. Mech. Eng. Sci.* **232** 2297–314.
[20] AL-Dujaili Z A, Jamali H U and Tolephih M H 2020 Calculation of Static and Dynamic Characteristics of a Finite Length Journal Bearing Considering 3D Misalignment *KJES* **0** 16-39.
[21] Pareja-Corcho J, Moreno A, Simoes B, Pedrera-Busselo A, San-Jose E, Ruiz-Salguero O and Posada J 2021 A Virtual Prototype for Fast Design and Visualization of Gerotor Pumps *Appl. Sci.* **11** 1190.
[22] Mancò S, Nervegna N, Rundo M, Armenio G, Pachetti C and Trichilo R 1998 Gerotor Lubricating Oil Pump for IC Engines *SAE Technical Paper*.
[23] Gamez-Montero P J and Codina E 2007 Flow characteristics of a trochoidal-gear pump using bond graphs and experimental measurement. Part 1 *Proc. Inst. Mech. Eng. Part J. Syst. Control Eng.* **221** 331–46.
[24] Gamez-Montero P J and Codina E 2007 Flow characteristics of a trochoidal-gear pump using bond graphs and experimental measurement. Part 2 *Proc. Inst. Mech. Eng. Part J. Syst. Control Eng.* **221** 347–63.